Estimate eddy diffusion coefficients from gravity wave vertical momentum and heat fluxes

Alan Z. Liu[1]

Received 29 January 2009; accepted 12 March 2009; published 17 April 2009.

[1] A method was presented to estimate the eddy momentum and thermal diffusion coefficients from the gravity wave momentum and heat fluxes based on linear saturation theory. This method was applied using the fluxes between 85–100 km altitude measured by a Na wind/temperature lidar at Starfire Optical Range, NM (35N, 106.5W). The seasonal and altitude variations of the diffusion coefficients and Prandtl number were estimated. It is found that both diffusion coefficients are small in spring and fall and large in winter and summer. The annual mean momentum diffusion coefficient is about 400 m^2/s between 85–100 km; the thermal diffusion coefficient decreases from 400 m^2/s at 85 km to 100 m^2/s at 100 km, resulting in a Prandtl number that increases with altitude from 1 to over 3. **Citation:** Liu, A. Z. (2009), Estimate eddy diffusion coefficients from gravity wave vertical momentum and heat fluxes, *Geophys. Res. Lett.*, *36*, L08806, doi:10.1029/2009GL037495.

1. Introduction

[2] The dissipation of atmospheric gravity waves (GWs) are one of the most important dynamic processes in the mesosphere and lower thermosphere (MLT) that controls the mean global circulation and thermal structure [*Fritts and Alexander*, 2003]. There are two primary mechanisms in GW dissipation that affect the middle atmosphere. One is the acceleration of mean wind and the dynamical heating/cooling due to vertical fluxes of momentum and heat. The other is the eddy mixing due to turbulence generated by GW breaking. Quantitatively estimating the eddy mixing is important because it is a major transport mechanism of all constituents in MLT region.

[3] Estimating eddy mixing is challenging because GWs vary over a large range of spatial and temporal scales, and their breaking and the resulting turbulence mixing processes are not well understood. In-situ measurement of turbulence in the MLT has been made in rockets experiments [e.g., *Bishop et al.*, 2004; *Chu et al.*, 2007; *Rapp et al.*, 2004], and the eddy diffusion can be estimated from the energy dissipation rate derived from these measurements. The turbulence energy dissipation can also be inferred from the spectral width of back-scattered radar signals [*Hocking*, 1983; *Lattecka et al.*, 2005]. Another approach by *Li et al.* [2007] is to infer eddy diffusion from an observed GW breaking event, based on the linear saturation theory (LST) [*Lindzen*, 1981]. The time evolution of a GW breaking event can be well described by the continuous measurement of wind and temperature with a Na wind/temperature lidar, which enables derivation of all the wave's intrinsic parameters necessary to infer the eddy diffusion.

[4] The LST describes the relationships between the background conditions in which a GW breaks and its effects on the background atmosphere through momentum and heat deposition and turbulence mixing. It is therefore possible to infer eddy diffusion from the momentum and heat fluxes. In this study, a new method is presented to infer the eddy diffusion coefficients from the momentum and heat fluxes measured by a Na wind/temperature lidar. Instead of focusing on a single GW event, this approach is based on mean flux measurements and provides a way to estimate diffusion coefficients at different seasons and altitudes in the mesopause region. The momentum and thermal diffusion coefficients are also estimated separately thus the variation of Prandtl number can be also be examined.

[5] A Na wind/temperature lidar can measure temperature and 3-D wind in the mesopause region at high resolutions, enough to resolve GWs at all scales that are significant in the region. The data collected using such a lidar by University of Illinois have been used to study GW momentum and heat fluxes [*Gardner and Liu*, 2007] (hereinafter referred to as GL07). In this study, the eddy diffusion coefficients were estimated from the momentum and heat fluxes derived by GL07 using lidar measurements made at Starfire Optical Range (SOR), New Mexico (35N, 106.5W).

[6] In the next section, the method and data will be described. The results will be presented in section 3, followed with discussion in section 4.

2. Method and Data

2.1. Linear Saturation Theory

[7] As a GW propagating upward from the lower atmosphere, its amplitude grows exponentially with altitude due to the decrease in atmospheric density. In the LST, it is assumed that at a certain altitude, this growth will lead to convective instability, when the potential temperature perturbation is large enough so its vertical gradient becomes negative. This is referred to as the "saturation altitude." Turbulence from such instability ensues and limits further growth of the GW amplitude. The limit of amplitude growth is accomplished through dissipation from turbulence mixing, which is represented as a diffusion term in both the momentum and thermodynamic equations. The wave breaking generates a net momentum deposition which results in the mean flow acceleration in the direction of wave propagation, and a non-zero downward heat flux that results in cooling of the atmosphere above.

[1]Department of Electrical and Computer Engineering, University of Illinois, Urbana, Illinois, USA.

0094-8276/09/2009GL037495$05.00

[8] When a GW reaches saturation, its wind perturbation u' is limited by the intrinsic phase speed $|c - \bar{u}|$ as

$$|u'| = |c - \bar{u}|, \tag{1}$$

where $\bar{u}$ is the mean horizontal wind in the direction of wave propagation, and c is the ground-based phase speed. The intrinsic frequency is $\omega = kc$, where k is the horizontal wavenumber. If we consider waves in the range $f^2 \ll \omega^2 \ll N^2$, where f and N are the inertial and buoyancy frequencies, respectively, the dispersion relation becomes

$$m = \frac{N}{\bar{u} - c}, \tag{2}$$

where m is the vertical wavenumber. The momentum flux above the saturation altitude is related to the background condition as [*Fritts*, 1984]

$$\overline{u'w'} = -\frac{1}{2}\frac{k}{N}(\bar{u} - c)^3, \tag{3}$$

where w' is the vertical wind perturbation. The momentum flux convergence is also related to the momentum diffusion coefficient K_M as [*Fritts*, 1984]

$$-\frac{1}{\bar{\rho}}\frac{\partial}{\partial z}\bar{\rho}\overline{u'w'} = \frac{N^2}{c - \bar{u}}K_M = -NmK_M, \tag{4}$$

where $\bar{\rho}$ is the background atmospheric density. The combined effects of momentum deposition and eddy diffusion on $\bar{u}$ result in an acceleration as

$$\frac{\partial \bar{u}}{\partial t} = -\frac{1}{\bar{\rho}}\frac{\partial}{\partial z}\bar{\rho}\overline{u'w'} + K_M\frac{\partial^2 \bar{u}}{\partial z^2}. \tag{5}$$

2.2. Momentum Diffusion Coefficient

[9] As shown in (4), the momentum flux is related to K_M in a simple way [*Weinstock*, 1982; *Fritts*, 1984; *Lindzen*, 1981], which provides a way to estimate K_M from the momentum flux. To apply this relation to a measured mean momentum flux, we need to consider the integral effects of all waves included in the measurement. In the right hand side of (4), we need a representative value of m. We choose $m^* = 2\pi/10$ km as a 'mean' value in our calculation based on (a) the lower limit of m in Na lidar data is about $2\pi/15$ km and (b) the m-spectra of the horizontal wind and temperature perturbations typically peak at $m = 2\pi/10$ km or less [*Fritts and Alexander*, 2003; *Gardner and Yang*, 1998].

[10] To relate the left hand side of (4) to the measured mean momentum flux, we write the momentum flux for waves in the direction between ϕ and $\phi + d\phi$ as

$$\overline{u'w'} = \Phi(\phi)d\phi, \tag{6}$$

where ϕ is the azimuth angle (defined as $\phi = 0$ towards north and increases clock-wise) and Φ is always positive. From (4) and (6), the average K_M can be written as

$$K_M = \frac{1}{Nm^*\bar{\rho}}\frac{\partial}{\partial z}\bar{\rho}\left[\frac{1}{2\pi}\int_0^{2\pi}\Phi(\phi)d\phi\right]. \tag{7}$$

If the mean momentum flux direction is ϕ_0, i.e.

$$F_M = \frac{1}{2\pi}\int_0^{2\pi}\Phi(\phi)\cos(\phi - \phi_0)d\phi, \tag{8}$$

then (7) can be written as

$$K_M = \frac{1}{Nm^*\bar{\rho}}\frac{\partial}{\partial z}\frac{\bar{\rho}F_M}{d}, \tag{9}$$

where

$$d = \frac{F_M}{\frac{1}{2\pi}\int_0^{2\pi}\Phi(\phi)d\phi} \tag{10}$$

is the so-called the polarization factor, which is a measure of the anisotropy of the GW field. $d = 0$ for an isotropic wave field and $d = 1$ for a monochromatic wave. In the real atmosphere, d is generally between 0 and 1 and can be estimated using a statistical method following *Vincent and Fritts* [1987]. First we calculate the Stokes parameters as

$$I = \overline{U'^2} + \overline{V'^2}, D = \overline{U'^2} - \overline{V'^2}, P = 2\overline{U'V'}, Q = 2\overline{U'V'_{+90}},$$

where U' and V' are the amplitudes of zonal and meridional wind perturbations, V'_{+90} is V' with a 90° phase shift obtained with the Hilbert transform, I is the total variance, D is the variance difference, P and Q are the in-phase and quadrature components of the complex correlation between the two components. Then d is calculated as

$$d = \left(D^2 + P^2 + Q^2\right)^{1/2}/I. \tag{11}$$

Note that when the GW field is close to isotropic, d is close to zero and K_M cannot be reliably obtained from (9).

2.3. Thermal Diffusion Coefficient

[11] In the original Lindzen's LST theory, the diffusion in momentum and thermal dynamic equations are the same, i.e. the Prandtl number $Pr = 1$. *Fritts and Dunkerton* [1985] and *Liu* [2000] extended this by considering a localized turbulence and derived that the wave heat flux is related to the thermal diffusion as

$$\overline{w'\theta'} \approx -(1 - 2\eta)\frac{\bar{\theta}}{2g}N^2K_H, \tag{12}$$

where $0 \le \eta \le 1$ is a localization measure of the turbulence and K_H is the thermal diffusion coefficient. (12) shows that a dissipating GW will produce a downward heat flux when the turbulence is uniform ($\eta = 0$). K_H can be estimated using (12) once the relative heat flux $\overline{w'\theta'}/\bar{\theta}$ is measured. Since we cannot determine the value of η, we will use $\eta = 0$, i.e. assume uniform turbulence when calculating K_H. This will underestimate K_H when the turbulence is localized ($\eta > 0$).

[12] The lidar measures temperature and vertical wind in geometric coordinates, so the covariance $\overline{w'T'}$ can be directly estimated. From the definition of potential temperature $\theta = T(p_0/p)^\kappa$, where $\kappa = R/C_p$, we can write

$$\frac{\overline{w'\theta'}}{\bar{\theta}} = \frac{\overline{w'T'}}{\bar{T}} - \kappa\frac{\overline{w'p'}}{\bar{p}}, \tag{13}$$

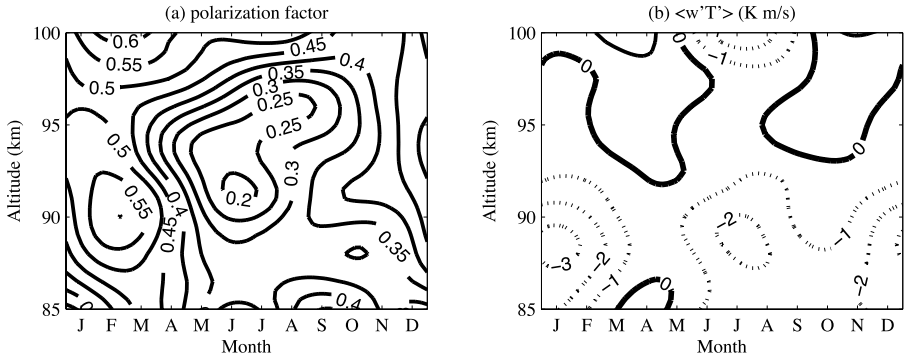

Figure 1. (a) Polarization factor d and (b) relative heat flux $\overline{w'\theta'}/\bar{\theta}$ as a function of month and altitude.

so the difference between $\overline{w'T'}$ and $\overline{w'\theta'}$ is related to the vertical energy flux $\overline{w'p'}$. Based on GW polarization relations, we can relate p', w' and T' for a single GW as [*Hines*, 1960; *Fritts and Alexander*, 2003]

$$\tilde{T} \approx \frac{N^2}{N^2-\omega^2}\left(iHm+\frac{1}{2}-\kappa\frac{\omega^2}{N^2}\right)\tilde{p},$$
$$\tilde{w} = \frac{i\omega g}{N^2-\omega^2}\left(iHm+\frac{1}{2}-\kappa\right)\tilde{p},$$

where $\tilde{T}$, $\tilde{w}$ and $\tilde{p}$ are complex amplitudes of $T'/\bar{T}$, w' and $p'/\bar{p}$, respectively. The energy flux is then

$$|\tilde{w}\tilde{p}^*| \approx -\frac{\omega g}{N^2 Hm}|\tilde{T}|^2.$$

Here again we assume $\omega^2 \ll N^2$, which is valid for waves with intrinsic period longer than 15 min, and $m \gg 1/2H$. The relative energy flux for an entire spectrum of waves is then

$$\frac{\overline{w'p'}}{\bar{p}} = \int_{m_1}^{m_2}\int_{\omega_1}^{\omega_2}|\tilde{w}\tilde{p}^*|d\omega dm \approx -\frac{g}{N^2 H}\iint\frac{\omega}{m}|\tilde{T}|^2 d\omega dm. \tag{14}$$

The suitable integration ranges for the lidar data are $\omega_1 = 2\pi/8$ hr, $\omega_2 = 2\pi/10$ min, $m_1 = 2\pi/15$ km and $m_2 = 2\pi/1$ km. The temperature power spectra obey the power law and their slopes have been derived by *Gardner et al.* [1998], who showed that for the SOR lidar temperature data, the vertical wavenumber spectrum follows $m^{-2.74}$ and the frequency spectrum follows $\omega^{-1.98}$ [see *Gardner et al.*, 1998, Table 1]. We can therefore write

$$|\tilde{T}|^2 = F_T(\omega, m) = \omega^{-1.98}m^{-2.74}F_0, \tag{15}$$

where F_0 is a constant. The total variance of the temperature is

$$\overline{T'^2} = \bar{T}^2\iint F_T(\omega,m)d\omega dm = F_0\iint\omega^{-1.98}m^{-2.74}d\omega dm. \tag{16}$$

Substituting (15) into (14) and using (16), we get

$$\frac{\overline{w'p'}}{\bar{p}} = -\frac{g\overline{T'^2}}{N^2 H}\frac{\iint\omega^{-0.98}m^{-3.74}d\omega dm}{\iint\omega^{-1.98}m^{-2.74}d\omega dm} \approx 1.346\frac{g\overline{T'^2}}{N^2 H\bar{T}^2}. \tag{17}$$

This relation is used to estimate the relative energy flux from temperature variance and then to calculated $\overline{w'\theta'}/\bar{\theta}$ from (13). Note that the absolute value of $\bar{\theta}$ is not needed in the calculation.

2.4. Lidar Data

[13] The lidar data from SOR include temperature and 3-D wind. They have a temporal resolution of 6 min and vertical resolution of 500 m so are sensitive to GWs with periods over 12 min and vertical wavelength over 1 km. The longest vertical wavelength resolved is limited by the 15 km thickness of the Na layer, and the longest period resolved is limited by the length of observation, typically 8 to 10 hours for a full night. There were 49 nights of data used in this study, that spread in every calendar month except in July throughout the year. More detailed description of the data are given by GL07. This dataset has been used to derive the GW momentum and heat fluxes given by GL07. In this study, the flux results from GL07 were used to derive eddy diffusion coefficients using the method derived in section 2.

[14] Because the mean flux estimate has large uncertainties due to large variabilities of temperature and wind, we focus only on the variation of diffusion coefficients on the seasonal scale. Follow the same data processing method as was used by GL07, all quantities were calculated as monthly mean which were then smoothed with a 5 km Hamming window in vertical, and fitted with the mean, annual and semi-annual oscillation to obtain the seasonal components. All the seasonal variations shown in this study were re-constructed from the fitted parameters.

3. Results

[15] Figure 1a shows the polarization factor d calculated according to (11). It is large from December to March, generally above 0.5, and small in summer with the minimum appears in June at 92 km with $d = 0.2$. This indicates that summer GW activity at SOR is more isotropic than in winter. Figure 1b shows the relative heat flux $\overline{w'\theta'}/\bar{\theta}$. It has large negative values below 92 km in the winter and the summer, as well as above 98 km in the summer. These are the regions where strong GW dissipation occurs which results in a downward heat flux [*Walterscheid*, 1981]. During the spring and fall seasons, the flux is small due to weak GW activity. Note that the coefficient in (17) used in the above calculation is dependent on the assumed ranges of m and ω, whose actual values vary for different nights

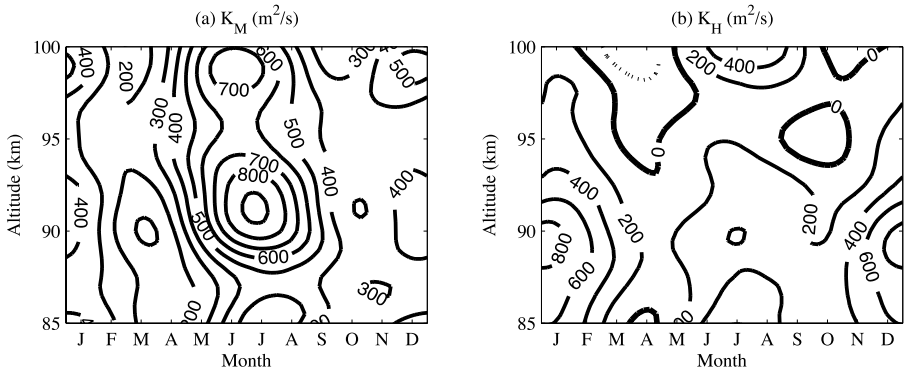

Figure 2. (a) Momentum diffusion coefficient K_M and (b) thermal diffusion coefficient K_H as a function of month and altitude.

because of changes in Na density thickness and hours of observation. Nevertheless, it doesn't change significantly (within about 15%) for reasonable ranges of m and ω. In addition, since the magnitude of $\overline{w'p'}$ is generally smaller than $\overline{w'T'}$ for dissipating GWs, the variation of the coefficient in (17) is of second order to the heat flux estimate.

[16] K_M was calculated from (9) and shown in Figure 2a. Its uncertainty was estimated from the uncertainties of momentum flux presented by GL07, and varies from $\sim$100 m^2/s in winter to $\sim$300 m^2/s in summer, mostly due to the variation of d. K_M has a distinctive maximum in the summer months with value exceeding 900 m^2/s, which is still meaningful even though the small d in summer results in a large uncertainty. The large value of K_M is mainly a result of large acceleration by GW momentum flux. As shown by GL07 (Figure 14), the acceleration is largest in summer in both zonal and meridional directions. K_M is smallest in spring with minimum below 100 m^2/s and is also small in fall, due to weak GW activities. In winter months, K_M has intermediate values around 400–500 m^2/s.

[17] K_H is shown in Figure 2b. Similar to K_M, K_H is smallest in spring and fall. The mean uncertainty of K_H is about 100 m^2/s. The small negative values in K_H is a result of positive $\overline{w'\theta'}$ shown in Figure 1b. It is mostly due to the large uncertainties at the top of Na layer where signals are low. The small K_H is mainly due to weak GW activity that results in less dissipation. K_H is largest in winter below 92 km, where GW dissipation is strongest. It also has two local maxima in summer below 87 km and above 98 km.

[18] The Prandtl number was calculated from the derived K_M and K_H as $Pr = K_M/K_H$. Their annual and vertical means are shown in Figure 3. In the annual means, while

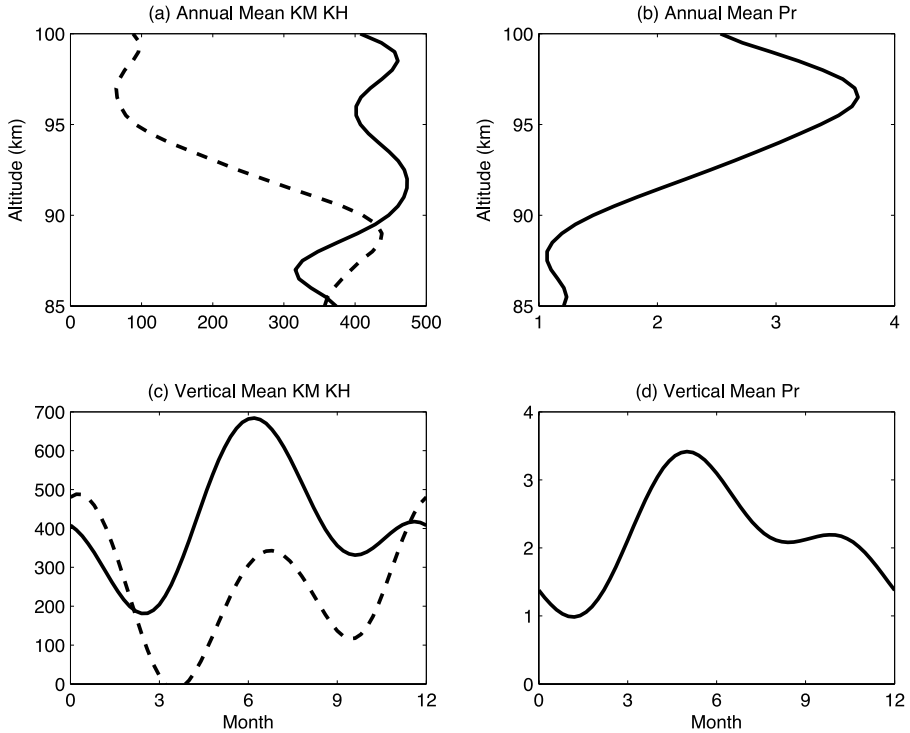

Figure 3. Annual means of (a) K_M (solid) and K_H (dash) and (b) Pr and vertical means of (c) K_M (solid) and K_H (dash) and (d) Pr.

K_M is nearly constant ($\sim$400 m^2/s) throughout the mesopause region, K_H decreases from $\sim$400 m^2/s at 85 km to $\sim$100 m^2/s above 95 km. As a result, *Pr* increases from $\sim$1 below 90 km to over 3 above 95 km. The vertical means indicate that both K_M and K_H have strong annual and semi-annual variations, with maxima around solstices and minima around equinoxes. The maximum K_M is in summer while the maximum K_H is in winter.

4. Discussion and Conclusions

[19] A new method was presented to estimate the eddy momentum and thermal diffusion coefficients from measured GW momentum and heat fluxes based on the LST. The advantage of this method is that it can provide an estimate of the seasonal and vertical variations of the mean K_M and K_H as well as the Prandtl number. The results can be compared with other inferred or measured diffusion coefficients to get better understanding of these important parameters.

[20] This method requires several important assumptions. First, the LST is a good description of the GW dissipation process. Second, in the mesopause region, most GWs are saturated. Even though these assumptions are mostly valid in the mesopause region, they are also the limitations of this method. We also have to assume that the turbulence is uniform (η = 0), which is often not true according to observations, and could affect the estimate of both K_M and K_H. In addition, when the mean wave field is near isotropic so the momentum flux in opposite directions cancel each other, the mean momentum flux is too small to be used to estimate K_M.

[21] The results based on SOR lidar data shows that K_M and K_H have large annual and semi-annual variations with maxima in solstice and minima in equinoxes. The annual mean K_M is nearly constant in vertical but K_H decreases with altitude. As a result, *Pr* increases from $\sim$1 below 90 km to over 3 above 95 km.

[22] **Acknowledgments.** Discussions with R. L. Walterscheid and Han-Li Liu are very helpful for this work and are much appreciated. This work was supported by NSF grants ATM-0804578 and ATM-0545704.

References

Bishop, R. L., M. F. Larsen, J. H. Hecht, A. Z. Liu, and C. S. Gardner (2004), TOMEX: Mesospheric and lower thermospheric diffusivities and instability layers, *J. Geophys. Res.*, *109*, D02S03, doi:10.1029/2002JD003079.

Chu, Y. H., C. L. Su, M. F. Larsen, and C. K. Chao (2007), First measurements of neutral wind and turbulence in the mesosphere and lower thermosphere over Taiwan with a chemical release experiment, *J. Geophys. Res.*, *112*, A02301, doi:10.1029/2005JA011560.

Fritts, D. C. (1984), Gravity wave saturation in the middle atmosphere: A review of theory and observations, *Rev. Geophys. Space Phys.*, *22*, 275–308.

Fritts, D. C., and M. J. Alexander (2003), Gravity wave dynamics and effects in the middle atmosphere, *Rev. Geophys.*, *41*(1), 1003, doi:10.1029/2001RG000106.

Fritts, D. C., and T. J. Dunkerton (1985), Fluxes of heat and constituents due to convectively unstable gravity waves, *J. Atmos. Sci.*, *42*, 549–556.

Gardner, C. S., and A. Z. Liu (2007), Seasonal variations of the vertical fluxes of heat and horizontal momentum in the mesopause region at Starfire Optical Range, New Mexico, *J. Geophys. Res.*, *112*, D09113, doi:10.1029/2005JD006179.

Gardner, C. S., and W. Yang (1998), Measurements of the dynamical cooling rate associated with the vertical transport of heat by dissipating gravity waves in the mesopause region at the Starfire Optical Range, New Mexico, *J. Geophys. Res.*, *103*, 16,909–16,926.

Gardner, C. S., S. J. Franke, W. Yang, X. Tao, and J. R. Yu (1998), Interpretation of gravity waves observed in the mesopause region at Starfire Optical Range, New Mexico: Strong evidence for nonseparable intrinsic (m, ω) spectra, *J. Geophys. Res.*, *103*, 8699–8713.

Hines, C. O. (1960), Internal atmospheric gravity waves at ionospheric heights, *Can. J. Phys.*, *38*, 1441–1481.

Hocking, W. K. (1983), On the extraction of atmospheric turbulence parameters from radar backscatter doppler spectra: I. Theory, *J. Atmos. Terr. Phys.*, *45*, 89–102.

Lattecka, R., W. Singer, and W. K. Hocking (2005), Measurement of turbulent kinetic energy dissipation rates in the mesosphere by a 3 MHz Doppler radar, *Adv. Space Res.*, *35*, 1905–1910.

Li, T., C. Y. She, H.-L. Liu, and M. T. Montgomery (2007), Evidence of a gravity wave breaking event and the estimation of the wave characteristics from sodium lidar observation over Fort Collins, CO (41°N, 105°W), *Geophys. Res. Lett.*, *34*, L05815, doi:10.1029/2006GL028988.

Lindzen, R. S. (1981), Turbulence and stress owing to gravity wave and tidal breakdown, *J. Geophys. Res.*, *86*, 9707–9714.

Liu, H.-L. (2000), Temperature changes due to gravity wave saturation, *J. Geophys. Res.*, *105*, 12,329–12,336.

Rapp, M., B. Strelnikov, A. Müllemann, F.-J. Lübken, and D. C. Fritts (2004), Turbulence measurements and implications for gravity wave dissipation during the MaCWAVE/MIDAS rocket program, *Geophys. Res. Lett.*, *31*, L24S07, doi:10.1029/2003GL019325.

Vincent, R. A., and D. C. Fritts (1987), A climatology of gravity wave motions in the mesopause region at Adelaide, Australia, *J. Atmos. Sci.*, *44*, 748–760.

Walterscheid, R. L. (1981), Dynamical cooling induced by dissipating internal gravity waves, *Geophys. Res. Lett.*, *8*, 1235–1238.

Weinstock, J. (1982), Nonlinear theory of gravity waves: Momentum deposition, generalized Rayleigh friction, and diffusion, *J. Atmos. Sci.*, *39*, 1698–1710.

A. Z. Liu, Department of Electrical and Computer Engineering, University of Illinois, 1308 West Main, Urbana, IL 61801, USA. (liuzr@illinois.edu)